JACS
JOURNAL OF THE AMERICAN CHEMICAL SOCIETY
Communication
pubs.acs.org/JACS

Simple Cubic Packing of Gold Nanoparticles through Rational Design of Their Dendrimeric Corona

Kiyoshi Kanie,*[,†] Masaki Matsubara,[†] Xiangbing Zeng,[‡] Feng Liu,[‡] Goran Ungar,*[,‡,§] Hiroshi Nakamura,[∥] and Atsushi Muramatsu[†]

[†]Institute of Multidisciplinary Research for Advanced Materials, Tohoku University, Katahira 2-1-1, Aoba-ku, Sendai 980-8577, Japan
[‡]Department of Materials Science and Engineering, University of Sheffield, Sheffield S1 3JD, U.K.
[§]School of Chemical and Biological Engineering, Seoul National University, Seoul 151-744, Korea
[∥]Toyota Central R&D Laboratories, Inc., 41-1 Yokomichi, Nagakute, Nagakute-Cho, Aichi-Gun, Aichi 480-1192, Japan

Supporting Information

ABSTRACT: The first simple-cubic liquid crystal was obtained by coating monodisperse Au nanoparticles (NPs) with a thick corona of amino-substituted organic dendrons. This unusual structure was determined by grazing-incidence diffraction and electron density reconstruction and explained by analyzing the radial density profile of the corona. Another novel structure is proposed for the phase preceding the cubic one: a hexagonal superlattice composed of alternating dense and sparse strings of Au NPs.

Fabrication of nanoparticle (NP)-based periodic structures has attracted considerable attention in materials science[1−3] because new synergistic functions could be derived from such structures. Top-down procedures could yield such structures,[4] but bottom-up approaches relying on self-organization are preferable. Considerable diversity of NP lattices has been obtained by self-organization of two different NP types.[5] Cubic arrangements of NPs have also been achieved by modification with self-complementary DNA[6,7] or a hydrophilic surfactant.[8] Moreover, an organic soft corona can promote periodic NP structures, and various calamitic[9−11] and dendritic[12−14] mesogens have been grafted onto NPs. As a result, liquid-crystalline (LC) phases with NPs in ordered arrays have been obtained.[1,15] Among organic soft materials, LC dendrons are the most likely to form spherical self-assembled aggregates. Such spherical objects can spontaneously form cubic,[16] tetragonal,[17] or even quasicrystalline[18] 3D structures. Modification by dendrons has already been applied to introduce self-assembling ability into functional materials such as light-harvesting antennae,[19] fullerenes,[20] and vitamins.[21]

As potential applications of hybrid NP-containing materials[1] depend critically on the detailed spatial arrangement, it is desirable to be able to design a wide range of lattices of NPs. One way to achieve this is to introduce anisotropy by coating the NPs with mesogenic ligands.[11] Even while staying with cubic or similar high symmetry, we may still wish to arrange the NPs on lattices other than body-centered (BCC) or face-centered cubic (FCC).[12] Thus, we set out to place the NPs into the center of a soft dendritic corona having a controllable radial density profile (RDP). It has been shown that the RDP is the key determinant of the type of packing for supramolecular dendrimers.[17] Here we used the convergent approach[22] for precise control of the divergent shape of the organic ligands to give the appropriate RDP and produce monodisperse gold NPs surrounded by a variety of double-shell dendritic coronas. This approach has considerable potential as a powerful alternative to the ligand-exchange method.[11,12] The new approach can be applied to various types of functional NPs, since the organic layer on their surfaces is readily tunable.

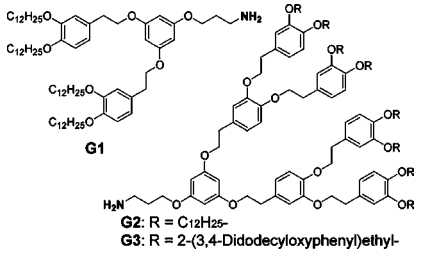

As dendrons, we synthesized the first-, second-, and third-generation phenethyl ether-type dendrons **G1**, **G2**, and **G3** with an amino group at the apex [for details, see the Supporting Information (SI)]. **G1**−**G3** themselves show a thermotropic LC hexagonal columnar phase (Col_h) upon heating (see Figures S1−S6 in the SI). The lattice constants (a) of the Col_h phases at 40 °C are 5.4, 5.6, and 6.1 nm for **G1**, **G2**, and **G3**, respectively. When they are heated, **G2** and **G3** form a liquid quasi-crystal (LQC)[18] phase via spontaneous formation of spherical assemblies. The LQC of **G2** is made up of spherical dendron aggregates of 9.8 nm diameter assuming a hard-sphere model (see the SI). Here we focused on encapsulating a hard NP core into soft assemblies of **G2** and **G3** whose size is compatible with that of the NP. The dendrons are attached as the outer corona through amidation to the carboxylic groups at the surface of the inner aliphatic corona encapsulating the NP. Purpose-designed CO_2H-modified monodisperse gold NPs **A1**, **A2**, and **A3** (see Figure 2b) were synthesized by the method of Zheng et al.[23] with some modifications using 12-dodecanethiol (DT) and 16-mercaptohexadecanoic acid (MHA) (see the SI). The initial DT/MHA molar ratio was fixed at 1/1, 3/2, and 4/1 for the preparation of **A1**, **A2**, and **A3**, respectively, to give dif-

Received: October 12, 2011
Published: December 19, 2011

   dx.doi.org/10.1021/ja2095816 | J. Am. Chem.Soc. 2012, 134, 808−811

ferent degrees of CO_2H modification. As shown by the transmission electron microscopy (TEM) images in Figure 1a–c,

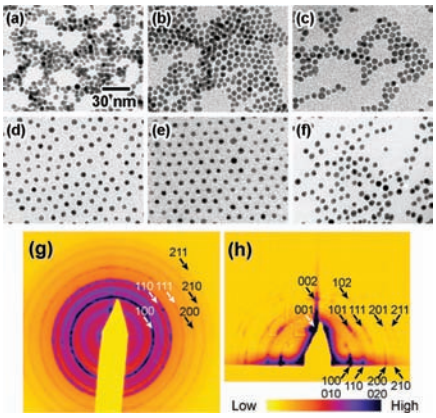

Figure 1. (a–f) TEM images of gold NPs: (a) **A1**; (b) **A2**; (c) **A3**; (d) **G2/A1**; (e) **G2/A2**; (f) **G2/A3**. The scale bar in (a) is common for (b–f). (g) SAXS pattern of **G2/A2** at 150 °C. (h) GI-SAXS profile of **G2/A2** on a Si substrate at 170 °C.

the shapes of the gold cores were close to spherical with narrow size distributions. The mean sizes and size distributions of the core parts of **A1**, **A2**, and **A3** were 5.9 ± 0.6, 6.8 ± 0.7, and 6.8 ± 0.8 nm, respectively. Modification of **A1**–**A3** to obtain dendron-modified gold NPs **G/A** was carried out by amidation reaction (see the SI). Complete removal of free **G** from **G/A** was ascertained by ^{1}H NMR and GPC measurements, while the formation of amide bonding was observed by IR spectra (see the SI). As a way of tailoring the corona, **G2/A1**, **G2/A2**, and **G2/A3** were prepared in this study. Furthermore, to investigate the effect of dendron generation on the ability of **A2** to self-organize, **G1/A2** and **G3/A2** were also synthesized using **G1** and **G3** dendrons. The methyl-to-carboxylic ratio DT/MHA on the surface of **A** was determined by ^{1}H NMR analysis after removal of the thiols from **A** using I_2 decomposition.[24] The peak at 0.9 ppm was attributed to the terminal methyl group of DT, and peaks around 1.2 ppm were assigned to methylene groups of both DT and MHA. By comparing the integral peak intensities, the DT/MHA modification molar ratios on the surfaces of **A1**, **A2**, and **A3** were determined as 10/8.0, 10/3.8, and 10/1.5, respectively (see the SI). Thermogravimetric analysis (TGA) showed that the weight losses of **A1**, **A2**, and **A3** were 9.3, 8.8, and 8.0%, respectively. These values were attributed to burning of DT and MHA. The numbers of DT (N_{DT}) and MHA (N_{MHA}) on a gold NP were calculated as described in the SI using the results of ^{1}H NMR and TGA measurements (Table 1). N_{MHA} could be

Table 1. Numbers and Ratios of DT, MHA, and G2

	DT/MHA[a]	N_{DT}[b]	N_{MHA}[b]	N_{G2}[b]	N_{G2}/N_{MHA}
A1	10/8.0	290	240	230	1.0
A2	10/3.8	600	220	280	1.3
A3	10/1.5	680	100	80	0.8

[a]Molar ratio of DT to MHA on the surface of a gold NP **A**. [b]Average number of DT, MHA, or **G2** molecules on the surface of a single **A**.

successfully controlled by adjusting the initial DT/MHA ratio. The weight losses in TGA were 34.9, 30.7, and 15.5% for **G2/A1**, **G2/A2**, and **G2/A3**, respectively (see the SI). These losses were due to burning off of DT, MHA, and **G2**. Thus, the weight fractions of **G2** in **G2/A1**, **G2/A2**, and **G2/A3**, as determined by subtracting the thiol component from the total weight loss, were calculated as 28.2, 24.0, and 8.2%, respectively. The numbers of **G2** molecules per **A1**, **A2**, and **A3** (N_{G2}) are also listed in Table 1, as are the ratios **G2/A1**, **G2/A2**, and **G2/A3** (see the SI). The fact that the N_{G2}/N_{MHA} ratios were close to 1 means that the amidation reaction with **G2** proceeded almost stoichiometrically. In this regard, the modification amount of dendron on **A** was precisely controlled by the present convergent-like process.

Figure 1d–f shows TEM images of the dendronized NPs **G2/A1**, **G2/A2**, and **G2/A3** cast from toluene. In the case of **G2/A2**, a well-ordered hexagonal monodomain with an interparticle distance of 14 nm formed (Figure 1e). The ability to self-organize seems to have been imparted by the dendritic corona. In **G2/A1**, a hexagonal polydomain structure was observed (Figure 1d), while only a random pattern was seen in **G2/A3** (Figure 1f). In the case of **G2/A3**, there were N_{G2} = 80 dendrons per **A3**, which is 3.5 times lower than in **G2/A2**. Thus, it would appear that dense grafting of **G2** is required to achieve a regular NP array. Furthermore, in the case of **G2/A2**, the gap between the NPs was spontaneously and precisely controlled to 7 nm (surface-to-surface) simply by casting and drying the solution, each NP being well isolated by the large interparticle distance. To date, NPs have been modified by various types of organic molecules, but the gap between the NPs is <3 nm in most cases.[25] For the development of NP-based materials such as quantum dots and magnetic memories,[26] not only precise control of large-area NP arrays but also perfect isolation of individual NPs by large gaps is required. Thus, the present method involving self-assembly of bulky dendrons, which gave a 2D hexagonal lattice of gold NPs having an interparticle distance of 14 nm and gaps of 7 nm between the surfaces of the NPs, may become a useful technique for the fabrication of NP-based devices. The effect of dendron generation on the 2D self-organization was also investigated using **G1/A2** and **G3/A2**. According to TEM, both systems formed only random arrays. The average interparticle distances for **G1/A2** and **G3/A2** were 9.2 and 12.6 nm, respectively. Thus, modification with **G1** and **G3** increased the distance between **A2** particles substantially but did not result in ordered arrays.

Next, we report on the 3D self-organization of the dendronized **G/A** NPs. Second-heating differential scanning calorimetry (DSC) traces for **G2/A** showed endotherms at 0 °C (**G2/A1**) and 9 °C (**G2/A2**) and a second broad endotherm at ~220 °C. In the temperature interval bounded by these transitions, the material is a viscous liquid; below it is rigid, and above it is fluid and subject to degradation. On the basis of experience with similar dendron systems, we attribute the lower endotherm to melting of the alkyl chains and the higher one to isotropization. No endotherms were seen for **G2/A3**. Temperature-dependent small-angle X-ray scattering (SAXS) analysis of **G2/A2** gave evidence of ordered nanostructures (see below). Other **G/A** systems produced only amorphous structures with short-range NP order. Only two broad SAXS peaks at ~10 and 5 nm were observed for **G2/A1** between 50 and 200 °C (Figure S16). **G2/A3** showed even less evidence of order: only scattering due to the NP form factor could be seen (Figure S17). Thus, the grafting density of **G2** on **A** plays a critical role in the formation of ordered structures. The effect of dendron generation on the LC structure was also investigated. Neither **G1/A2** nor **G3/A2** showed order (see the SI). Thus, the general ability to form ordered arrays in the bulk parallels that on the surface (Figure 1d–f).

dx.doi.org/10.1021/ja2095816 | J. Am. Chem.Soc. 2012, 134, 808–811

G2/A2 exhibited a series of moderately sharp SAXS peaks in a wide range from room temperature to 200 °C (Figure S12), indicatiing that several phases, some metastable, coexist. Therefore the sample was annealed at increasing temperatures. From room temperature to 130 °C, two relatively broad rings remained dominant, with their corresponding spacings in a ratio close to $3^{1/2}$ (see Figure 4a). We will return to this phase below. Upon further annealing at 150 °C, a series of sharp Bragg rings developed, with their corresponding reciprocal spacings in the ratio $1{:}2^{1/2}{:}3^{1/2}{:}4^{1/2}{:}5^{1/2}{:}6^{1/2}$, as shown in Figure 1g (the two broader rings from the previous phase are still visible). Although the absence of the seventh Bragg ring suggests the simple cubic phase (see Figure S12; the arrow shows where that peak would have been if it had been observed), we cannot rely on this evidence alone because the form factor approaches zero in this region and all of the reflections become weak. Therefore, we tried to obtain an oriented sample in order to establish this unequivocally (i.e., to eliminate the possibility of BCC, which would give the same ratio of spacings). Thus, grazing-incidence SAXS (GI-SAXS) experiments were carried out on a thin film of **G2/A2** on a Si substrate. Good orientation was achieved after annealing at 170 °C and subsequent cooling (Figure 1h). The spatial arrangement of the reflections confirmed unequivocally their indexing as (100), (110), (111), ... of a simple-cubic (SC) lattice rather than (110), (200), ... of a BCC lattice. For example, if the first reflection, at the scattering vector q_1, were indexed as $(110)_{BCC}$ rather than $(100)_{SC}$, then the distance between the layer lines in the pattern would have been $2^{1/2}q_1$ rather than the observed q_1. With no systematic extinctions, space group $Pm\bar{3}m$ was selected. Diffraction intensities were measured (see Table S2) and used in constructing the 3D electron density map presented in Figure 2a (for details, including the volume fraction vs density

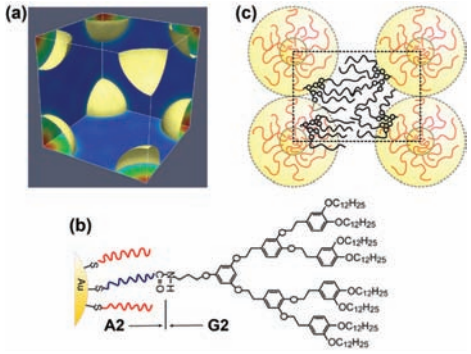

Figure 2. (a) 3D electron density map of a unit cell of the $Pm\bar{3}m$ SC phase reconstructed from the diffraction pattern in Figure 1g (blue, lowest density; red, highest density). The isoelectron surface delimits the spherical region of highest density (i.e., gold); organic matter fills the continuum. (b) Schematic of part of the double corona of a **G2/A2** NP. (c) (110) section through the unit cell.

histogram, see the SI); this map shows that the spherical high-density (i.e., gold) regions are located only at the corners of a cubic unit cell having a = 12.5 nm. We simulated the diffraction intensities using a model of solid spheres placed at the corners of the cubic cell and obtained an excellent fit with experiment for spheres of diameter 6.25 nm (Table S2), which is also in good agreement with values from TEM (6.8 nm) and the 69.3% weight retention after the organic component was burned off (the corresponding 9.5 vol % for Au indicates an Au NP diameter of 7.0 nm).

To our knowledge, this is the first example of a self-assembled SC array of spherical NPs, although close-packed cube-shaped NPs with a thin corona have previously been seen to pack on a SC lattice.[27] It is also the first example of a SC phase in a liquid crystal, either thermotropic[28] or lyotropic.[29] We are aware of only one example in block copolymers.[30] The absence of previous examples of SC packing is not surprising in the case of NPs, as SC packing offers a very low packing efficiency for spheres. In the case of dendrimers, the observed prevalence of $Pm\bar{3}m$, $Pm\bar{3}n$ (BCC), and $P4_1mnm$ phases has been interpreted in terms of the RDP of the soft corona, defined as RDP = $A(r)$, where A is the cross-sectional area of the dendron as a function of the distance r from its apex. A given dendrimer tries to find a lattice for which the rate of space filling by growing nonoverlapping spheres, dV/dr, most closely matches its RDP. Here, V is the occupied volume and r the sphere radius. A similar approach was also used to explain the occurrence of different bicontinuous cubic LC phases.[31] In Figure 3, numerically calculated scaled dV/dr functions are

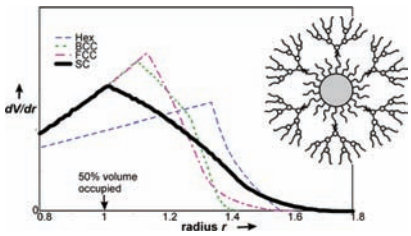

Figure 3. Rates of volume increase dV/dr as functions of radius r for growth of nonoverlapping spheres arranged on common cubic lattices: BCC = body-centered, FCC = face-centered, SC = simple-cubic. Hex denotes the analogous curve for cylinders on 2D hexagonal lattice. The curves are normalized to the same total volume and 50% of the occupied volume. Inset: schematic structure of **G2/A2**.

plotted against r for BCC, FCC, and SC as well as for the case of growing cylinders on a hexagonal 2D lattice. The curves for $Pm\bar{3}m$ and $P4_1mnm$ (not shown) are not too dissimilar from that for BCC. While spheres grow freely, $dV/dr \propto r^2$, but the curves differ once the spheres clash. The SC curve differs significantly from the others, as the drop in dV/dr starts significantly earlier and continues for longer. This is because the clash occurs at a relatively low occupied volume, whereas the volume is not completely filled until r almost doubles. This provides a clue to why **G2/A2** chooses SC. As the DT/MHA ratio is 10/3.8, only one in 3.6 chains of the inner corona continues to the outer **G2** corona. This would produce a sharp drop in dV/dr for an actual **G2/A2** sphere, as depicted schematically in the Figure 3 inset and Figure 2b. Considerably simplified, one could say that the touching spheres consist of the gold core and the inner DT/MHA corona, while the dendron parts serve to fill the remaining volume, including interstices (see the schematic in Figure 2c).

We now return to the phase that develops on heating and annealing at 130 °C and is the precursor to the SC phase. Its SAXS pattern consists of only two relatively broad rings with spacings of 17.7 and 10.2 nm (i.e., in the ratio $3^{1/2}$). It is difficult to be certain about a structure on the basis of such scarce data, and the one proposed here is rather speculative. We assume a 2D hexagonal superlattice (HS), with the two reflections indexed as (10) and (11). One of the two possible electron density maps reconstructed from these two reflections is shown in Figure 4c, and the alternative is shown in Figure S14a.

dx.doi.org/10.1021/ja2095816 | J. Am. Chem.Soc. 2012, 134, 808–811

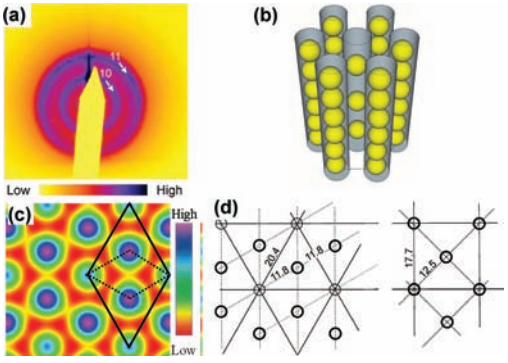

Figure 4. The HS in **G2/A2**. (a) SAXS pattern at 130 °C. (b) Model. (c) Electron density map projected along the sixfold axis. (d) Comparison of HS and SC (top view). Bold (thin) circles = dense (dilute) columns; thin circles = distances (in nm) are projections on the *xy* plane.

The map in Figure 4c is preferred, as it can be interpreted as representing columns of NPs where for every two densely packed columns there is a diluted one containing half the number of NPs (Figure 4b). The interparticle distances compare well with those in the SC phase (Figure 4d). In the main, the SAXS pattern of unannealed **G2/A2** (Figure 4a) may tentatively be attributed to a poorly developed 2D hexagonal phase with the strongest three peaks indexed as (10), (11), and (20). Its unit cell (a = 11.8 nm; dotted in Figure 4c) is equivalent to the subcell of the full cell of the HS (a = 20.4 nm; solid lines). The HS may provide a better match for the RDP of **G2/A2** than simple hexagonal lattice and may be a convenient intermediate step on the way to the SC.

In summary, dendron-modified gold NPs **G/A** have been fabricated through surface modification of monodisperse gold NPs with the quasicrystal-forming dendron **G2** via convergent-like synthesis. They can be regarded as organic–inorganic hybrid dendrimers with thermotropic LC behavior. The effects of dendron generation and surface coverage by dendrons on the mode of self-organization of NPs have been investigated for the first time. The gold NPs were found to assemble on a highly ordered SC lattice, space group $Pm\bar{3}m$. This is the first SC liquid crystal, thermo- or lyotropic, and represents the first example of SC self-assembly of spherical NPs. Its formation has been interpreted in terms of the match of the RDP of the soft corona with dV/dr for the SC lattice. An unusual hexagonal superlattice arrangement of dense and sparse NP strings is proposed for the phase leading to the SC phase. Further studies using quantum dots and magnetic NPs are now in progress.

■ ASSOCIATED CONTENT

Supporting Information

Preparation and characterization details. This material is available free of charge via the Internet at http://pubs.acs.org.

■ AUTHOR INFORMATION

Corresponding Author

kanie@tagen.tohoku.ac.jp; g.ungar@shef.ac.uk

■ ACKNOWLEDGMENTS

This work was financially supported by JSPS [Grants-in-Aid for Scientific Research (A) 16685018, 19685017, and 22685019], the METI & NEDO Super Hybrid Materials Development Project, the European FP7 Project NANOGOLD (NMP3-SL-2009-228455), and the WCU Program through the NRF of Korea funded by the Ministry of Education, Science and Technology (R31-10013). For help with the synchrotron experiments we thank Prof. S. Collins and Dr. A. Bombardi (beamline I16) and Drs. N. Terrill and J. Hiller (I22) at the Diamond Light Source.

■ REFERENCES

(1) Draper, M.; Saez, I. M.; Cowling, S. J.; Gai, P.; Heinrich, B.; Donnio, B.; Guillon, D.; Goodby, J. W. *Adv. Funct. Mater.* **2011**, *21*, 1260.
(2) Boettcher, S. W.; Strandwitz, N. C.; Schierhorn, M.; Lock, N.; Lonergan, M. C.; Stucky, G. D. *Nat. Mater.* **2007**, *6*, 592.
(3) Miyake, M.; Chen, Y. C.; Braun, P. V.; Pierre, W. *Adv. Mater.* **2009**, *21*, 3012.
(4) Campbell, M.; Sharp, D. N.; Harrison, M. T.; Denning, R. G.; Turber, A. J. *Nature* **2000**, *404*, 53.
(5) Shevchenko, E. V.; Talapin, D. V.; Kotov, N. A.; O'Brien, S.; Murray, C. B. *Nature* **2006**, *439*, 55.
(6) Nykypanchuk, D.; Maye, M. M.; Lelie, D.; van der Gang, O. *Nature* **2008**, *451*, 549.
(7) Park, S. Y.; Lytton-Jean, A. K. R.; Lee, B.; Weigand, S.; Schatz, G. C.; Mirkin, C. A. *Nature* **2008**, *451*, 553.
(8) Fan, H.; Leve, E.; Gabaldon, J.; Wright, A.; Haddad, R. E.; Brinker, C. J. *Adv. Mater.* **2005**, *17*, 2587.
(9) Kanie, K.; Muramatsu, A. *J. Am. Chem. Soc.* **2005**, *127*, 11578.
(10) Kanie, K.; Sugimoto, T. *J. Am. Chem. Soc.* **2003**, *125*, 10518.
(11) Zeng, X.; Liu, F.; Fowler, A. G.; Ungar, G.; Cseh, L.; Mehl, G. H.; Macdonald, J. E. *Adv. Mater.* **2009**, *21*, 1746.
(12) Donnio, B.; García-Vázquez, P.; Gallani, J. L.; Guillon, D.; Terazzi, E. *Adv. Mater.* **2007**, *19*, 3534.
(13) Marx, V. M.; Girgis, H.; Heiney, P. A.; Hegmann, T. *J. Mater. Chem.* **2008**, *18*, 2983.
(14) Wojcik, M.; Lewandowski, W.; Matraszek, J.; Mieczkowski, J.; Borysiuk, J.; Pociecha, D.; Gorecka, E. *Angew. Chem., Int. Ed.* **2009**, *48*, 5167.
(15) Bisoyi, H. K.; Kumar, S. *Chem. Soc. Rev.* **2011**, *40*, 306.
(16) Hudson, S. D.; Jung, H.-T.; Percec, V.; Cho, W.-D.; Johansson, G.; Ungar, G.; Balagurusamy, V. S. K. *Science* **1997**, *278*, 449.
(17) Rosen, B. M.; Wilson, D. A.; Wilson, C. J.; Peterca, M.; Won, B. C.; Huang, C.; Lipski, L. R.; Zeng, X.; Ungar, G.; Heiney, P. A.; Percec, V. *J. Am. Chem. Soc.* **2009**, *131*, 17500.
(18) Zeng, X.; Ungar, G.; Liu, Y.; Percec, V.; Dulcey, A. E.; Hobbs, J. K. *Nature* **2004**, *428*, 157.
(19) Jiang, D.-L.; Aida, T. *Nature* **1997**, *388*, 454.
(20) Sawamura, M.; Kawai, K.; Matsuo, Y.; Kanie, K.; Kato, T.; Nakamura, E. *Nature* **2002**, *419*, 702.
(21) Kato, T.; Matsuoka, T.; Nishii, M.; Kamikawa, Y.; Kanie, K.; Nishimura, T.; Yashima, E.; Ujiie, S. *Angew. Chem., Int. Ed.* **2004**, *43*, 1969.
(22) Hawker, C. J.; Fréchet, J. M. J. *J. Am. Chem. Soc.* **1990**, *112*, 7638.
(23) Zheng, N.; Fan, J.; Stucky, G. D. *J. Am. Chem. Soc.* **2006**, *128*, 6550.
(24) Templeton, A. C.; Hostetler, M. J.; Warmoth, E. K.; Chen, S.; Hartshorn, C. M.; Krishnamurthy, V. M.; Forbes, M. D. E.; Murray, R. W. *J. Am. Chem. Soc.* **1998**, *120*, 4845.
(25) Kwon, S. G.; Hyeon, T. *Acc. Chem. Res.* **2008**, *41*, 1696.
(26) Sun, S.; Murray, C. B.; Weller, D.; Folks, L.; Moser, A. *Science* **2000**, *287*, 1989.
(27) Demortière, A.; Launois, P.; Goubet, N.; Albouy, P.-A.; Petit, C. *J. Phys. Chem. B* **2008**, *112*, 14583.
(28) Ungar, G.; Tschierske, C.; Abetz, V.; Holyst, R.; Bates, M. A.; Liu, F.; Prehm, M.; Kieffer, R.; Zeng, X. B.; Walker, M.; Glettner, B.; Zywocinski, A. *Adv. Funct. Mater.* **2011**, *21*, 1296.
(29) Hassan, S.; Rowe, W.; Tiddy, G. J. T. In *Handbook of Applied Surface and Colloid Chemistry*; Holmberg, K., Ed.; Wiley: Chichester, U.K., 2002; Vol. *1*, p 465.
(30) Meng, F. L.; Zheng, S. X.; Li, H. Q.; Liang, Q.; Liu, T. X. *Macromolecules* **2006**, *39*, 5072.
(31) Zeng, X. B.; Ungar, G.; Impéror-Clerc, M. *Nat. Mater.* **2005**, *4*, 562.